Constraining the exchange through the strait of Bab el Mandab

by

Samah Serelkhatem Abdelkareem Satti

A thesis submitted in partial fulfillment for the
degree of Master of Science in Physical Oceanography
at the

UNIVERSITY OF BERGEN
Geophysical Institute

October 2012

UNIVERSITY OF BERGEN

Faculty of Mathematics and Natural Sciences
Geophysical Institute

Master of Science in Physical Oceanography

by

Samah Serelkhatem Abdelkareem Satti

Abstract

The strait of Bab el Mandab connects the Red Sea with the Indian ocean via the Gulf of Aden. The mean circulation at the strait is a three-layered exchange. The circulation in the Red Sea is understood to be driven by the air - sea fluxes, such as, evaporation and heat loss. We modify a thermohaline circulation (THC) model originally developed for the Nordic Seas and Arctic Mediterranean by Eldevik and Nilsen (2010) to constrain the variability of THC at Bab el Mandab. We find that the surface and intermediate inflow branches are sensitive to change in heat and evaporation, but the deep outflow is predominantly sensitive to evaporation only. The model suggests that the circulation is relatively sensitive to thermohaline change (about 17% - 44% of the mean flow). The model estimates a weaker thermohaline exchange at Bab el Mandab in 2050 using projected future climate change.

Acknowledgements

I would never have been able to finish my thesis without help from many people. First of all I would like to thank my supervisor Tor Eldevik and my co-supervisor Knut Barthel for the guidance, help, advice and suggestions. I would also like to acknowledge Asgeir Sorteberg for the good help and information about climate change in tropical region. I also thank all the staff at the Geophysical Institute. I am most grateful to Norad's Programme for Master Studies (NOMA) for the support during my master study.

Many thank go to all friends in Bergen for helpful and support. I am very grateful to my classmates, thanks for friendship and memories. Especial thank go to my MUM Ebtesam, my DAD Serelkhatem and my family for the personal support and prayers.

Contents

List of Figures

List of Tables

to my parents, sister

brothers, friends

Chapter 1

Introduction

The Red Sea is an enclosed basin; and the strait of Bab el Mandab connect the Red Sea to the Indian Ocean via Gulf of Aden. The Red Sea has a high rate of evaporation that drives the estuarine circulation which result high salinity outflow through the strait (Smeed, 2004). This outflow has a large effect upon the thermohaline circulation of the Indian Ocean (Schott and McCreary Jr, 2001; Beal et al., 2000).

There is an exchange in the flow through the Bab el Mandab strait, this exchange has a seasonal variability as a result of the monsoon climate (Smeed, 2004). During the winter (October - May), the flow is two layer exchange: warm fresh water flows into the Red Sea in the surface layer, and cool saline water flows out of the Red Sea (in the Gulf of Aden) in the lower layer (Smeed, 2004). In summer (June - September), there is a three layer flow: both the surface and deep layer outflow from the Red Sea and intermediate layer flows into the Red Sea from Gulf of Aden,(see Figure 1.1). The annual mean of the exchange flow is characterized by three layers: warm fresh surface and intermediate layer that flow into the Red Sea, and a cool saline outflow from the Red Sea into the Gulf of Aden, (see Figure 1.2) (Tragou et al., 1999).

According to Tragou et al. (1999) the circulation through the strait of Bab el Mandab is drived by air - sea fluxes such as evaporation and heat loss. We present a thermohaline circulation (THC) model to constrain the annual variability at the

strait. The main purpose of the model is to constrain the variability and strength of the thermohaline circulation across the Bab el Mandab.

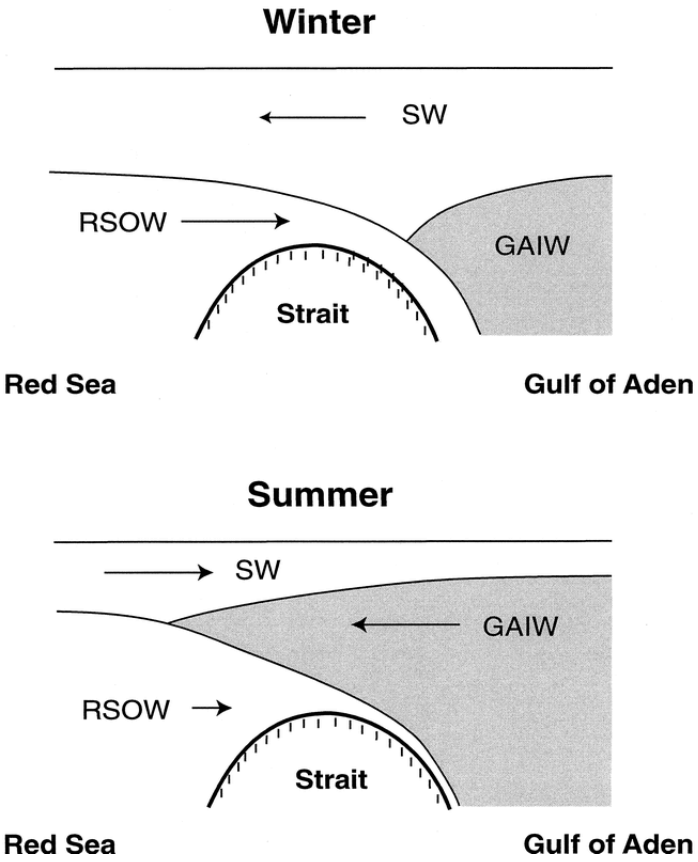

FIGURE 1.1: The exchange at Bab el Mandab in winter and summer, SW is surface water, GAIW is Gulf of Aden intermediate water, and RSOW is Red Sea outflow water, figure taken from (Smeed, 2004).

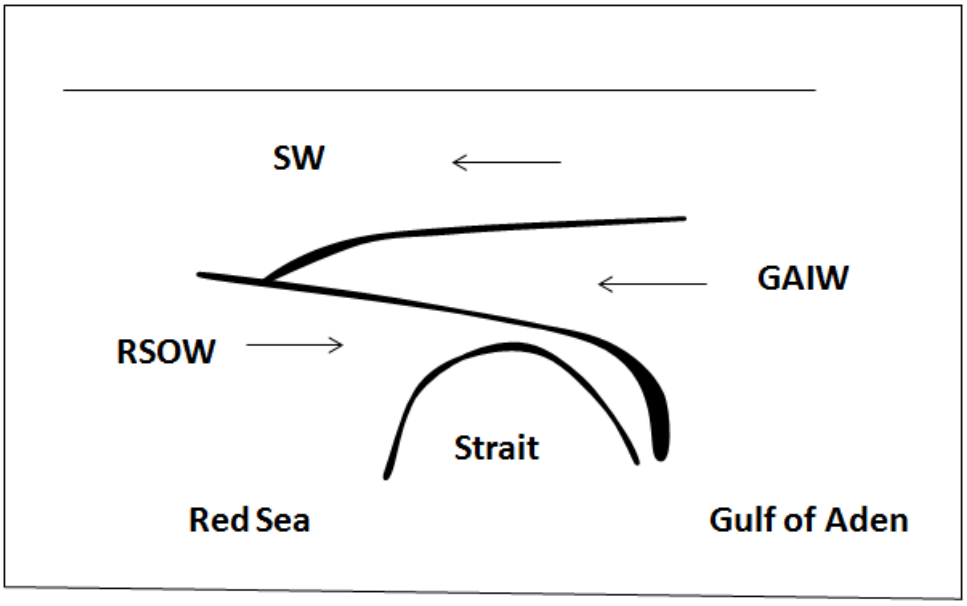

FIGURE 1.2: The annual mean exchange at Bab el Mandab, SW is surface water, GAIW is Gulf of Aden intermediate water, and RSOW is Red Sea outflow water.

Chapter 2

Area of study

2.1 The Red Sea

The Red Sea is a long narrow basin; it's almost enclosed and has just one connection to the global ocean, which is the Indian Ocean (Gulf of Aden) via the strait of Bab el Mandab in the south of the Red Sea (Siddall et al., 2002a). In the north, the sea divides into two narrow arms that flank the Sinai Peninsula which are the Gulf of Suez and the Gulf of Aqaba. The Red Sea lies between the Arabian Peninsula and Africa, extending from about 12.5° N - 30° N. The basin is 2000 km long and 280 km wide and the average depth is about 480 m (Degens and Ross, 1969; Siddall et al., 2002b). The Red Sea bordered by Egypt, Sudan, Eritrea and Djibouti on the west, and Yemen and Saudi Arabia on the east (Figure 2.1) (Saad, 2010).

The Red Sea has a highest surface salinity of the world's ocean; there is a net evaporation of about 1.5 m/yr from the sea surface (Tragou et al., 1999), and the precipitation is small, estimates ranging from 0.5 - 0.15 m/yr (Morcos, 1970; da Silva et al., 1994).

FIGURE 2.1: The location of the Red Sea Wikipedia (2012).

2.2 Gulf of Aden

The Gulf of Aden is geologically a young ocean basin. It is located in the Arabian Sea between Yemen, on the south coast of the Arabian Peninsula, and the Somalia in the Horn of Africa. In the northwest it is connected with the Red Sea through the strait of Bab el Mandab.

The length of the Gulf of Aden is approximately 920 km and the width 480 km. It has high sufrace temperature (25 - 31°C) (Britannica, 2012). The flow pattern of the Gulf of Aden is very much influenced by the monsoon winds, which is also reflects the seasonal exchange at Bab el Mandab.

2.3 Bab el Mandab

The water masses exchange through the straits which is Bab el Mandab connects semi-enclosed basins with large water bodies (oceans). These exchange processes depend on the flow dynamics that are usually very complex in the straits. Such as in the case of the strait of Bab el Mandab (Jarosz, 1997).

The Bab el Mandab is a strait 150 km long and 32 km wide that connects the Red Sea to the Indian Ocean via Gulf of Aden. The shallowest section of Bab el Mandab strait consists of Hanish sill and is located 150 km north of the narrowest passage (Figure 2.2) , the depth in the sill is about 137 m and the total width is 110 km. In the Perim Narrows the total width is only 18 km, and the depth is about 300 m in the central channel (Siddall et al., 2002b).

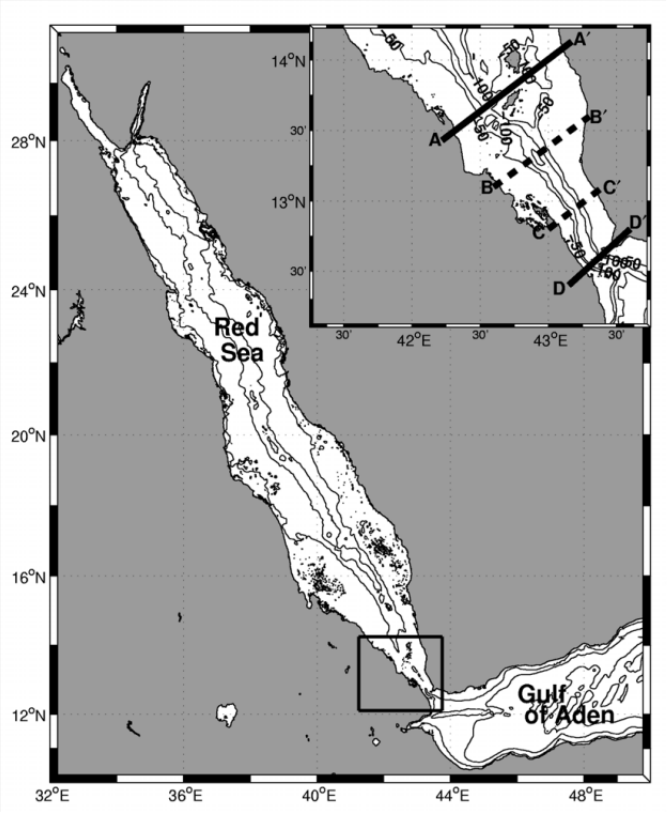

FIGURE 2.2: The strait of Bab el Mandab, the cross-section of Bab el Mandab: AA' is at Hanish sill and DD' is at Perim Narrows, taken from (Siddall et al., 2002b).

Chapter 3

Methodology

The Red Sea connects with the open ocean via the narrow and shallow strait of Bab el Mandab. The circulation of the Red Sea is believed to be driven mainly by the annual mean surface buoyancy loss caused by the high evaporation rate(Tragou et al., 1999). And also the seasonally changing wind patterns at the southern end of the sea are believed to affect the buoyancy-driven circulation (Tragou et al., 1999).

There are three main water masses involved in the circulation and exchange of the Red Sea. There is inflow of both surface and intermediate layer that is balanced by evaporation and consequently a very saline outflow at depth, the three water masses that characterise the THC (ThermoHaline Circulation) of the Red Sea, see Figure 3.1. The monthly mean values of the volume transports for the three layers, and temperatures and salinities over each layer are listed in Table 3.1, and the annual mean listed in Table 3.2.

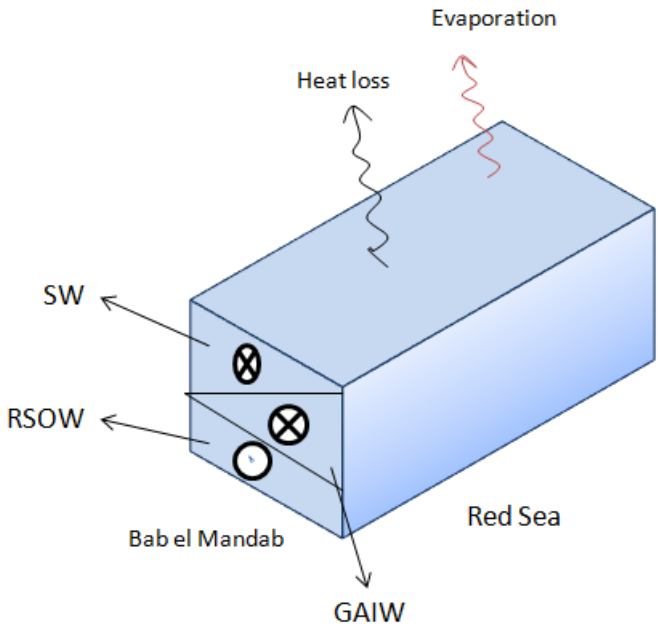

FIGURE 3.1: Conceptual sketch of the three-layered THC model. SW is upper layer in the Red Sea, GAIW is intermediate layer in the Red Sea, RSOW is lower layer of the Red Sea.

TABLE 3.1: Monthly mean volume transports, temperatures, and salinities for the three layers, taken from (Tragou et al., 1999).

Month	u_1 (Sv)	u_2 (Sv)	u_3 (Sv)	t_1 °C	t_2 °C	t_3 °C	s_1 (psu)	s_2 (psu)	s_3 (psu)
Jan	0.57		-0.55	25.0		22.5	37.7		40.3
Feb	0.40		-0.38	24.9		22.7	37.8		40.2
Mar	0.57		-0.55	25.2		22.5	37.9		40.1
Apr	0.42		-0.40	26.0		22.5	38.2		40.6
May	0.38		-0.36	26.3		22.5	38.3		40.5
Jun	-0.06	0.31	-0.23	29.5	25.1	22.3	37.2	39.0	40.6
Jul	-0.20	0.25	-0.03	30.7	24.9	22.5	37.5	38.6	40.3
Aug	-0.21	0.33	-0.10	30.9	24.2	22.4	37.8	38.0	40.4
Sep	-0.09	0.20	-0.09	31.2	22.9	22.0	38.5	37.8	40.5
Oct	0.52		-0.50	26.7		22.0	37.8		40.4
Nov	0.57		-0.55	26.6		20.6	38.0		40.3
Dec	0.51		-0.49	25.9		22.1	37.7		40.4

TABLE 3.2: Annual mean volume transports, temperatures, and salinities for the three layers, based on Table 3.1.

U_1 (Sv)	U_2 (Sv)	U_3 (Sv)	T_1 °C	T_2 °C	T_3 °C	S_1 (psu)	S_2 (psu)	S_3 (psu)
0.28	0.09	-0.35	27.4	24.3	22.2	37.9	38.4	40.4

As reviewed by Tragou et al. (1999), in Table 3.1 the monthly mean volume transport (in Sv; 1 Sv = $10^6 \mathrm{m}^3\mathrm{s}^{-1}$) for the upper layer U_1 have been estimated by Patzert (1974) using ship drift observation, and for the intermediate inflow layer U_2 (from Jul to Sep) from Maillard and Soliman (1986), the deep outflow layer U_3 from Tragou et al. (1999). And the monthly mean temperature (°C) and salinities

(psu) are taken from Levitus and Boyer (1994). In Table 3.2 we estimated the annual mean volume transports, temperatures, and salinities for the three layers.

The value of mean annual temperatures and salinities in Table 3.2 are plotted in TS - plot in Figure 3.2. The buoyancy forcing (F,Q) transforms the surface and intermediate water into the deep outflow (mixing line). F ,Q are evaporation and heat loss ,respectively, and will be further defined in relation to Equation 3.5.

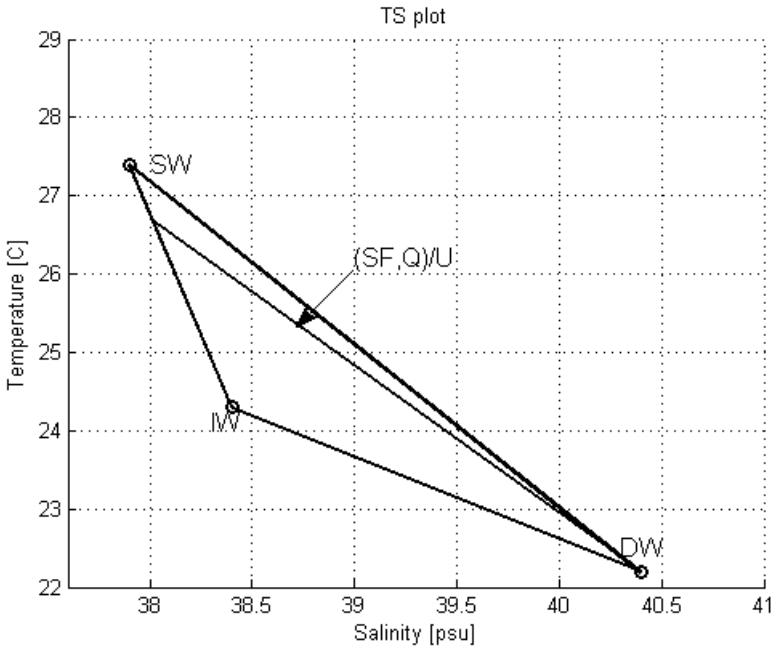

FIGURE 3.2: TS - plot of Bab el Mandab. SW is surface water, IW is intermediate water, DW is deep water, S is reference salinity of the Red Sea, U is volume transport of the deep outflow.

To constrain the exchange at Bab el Mandab analytically we will set up THC model but firstly set up estuarine circulation model.

3.1 Estuarine circulation

Estuarine circulation is controlled by many events of the ocean such as the inflow of river, the tides, rainfall, and the evaporation. In the Red Sea, the estuarine circulation occure because the evaporation rate exeed fresh-water input, this circulation is two layer exchange flow lasts from October to May with a relatively fresh surface inflow and a very saline deep outflow (Sofianos and Johns, 2002).

To estimate estuarine circulation from evaporation we will use conservation of volume and salt equations (Knudsen equations). For the Red Sea the Knudsen equations are:

$$U_{in} + U_{out} = F \tag{3.1a}$$

$$S_{in}U_{in} + S_{out}U_{out} = 0 \tag{3.1b}$$

where F is net of evaporation, U_{in} is the annual mean volume transport of the inflow at the surface (upper layer), U_{out} (U_3) is the volume transport of the outflow at the depth (lower layer), S_{in} (S_1) is the salinity of the upper layer, and S_{out} (S_3) is the salinity of the lower layer. The flow into the Red Sea is defined as positive while the flow out of the Red Sea is negative.

To get an estimate for the evaporation rate F we will solve the Equation 3.1. First solve Equation 3.1b by obtaining the value of salinities and volume transport of the lower layer from Table 3.2, the volume transport of lower layer $U_{out} = 0.37$ Sv. Then from Equation 3.1a the annual mean evaporation rate is 20 mSv.

$$F^{ref} = 20 \text{ mSv}$$

By solving Knudsen equations (Eq. 3.1) we get:

$$U_{in} = \frac{S_{out}F}{\Delta S} \tag{3.2a}$$

$$U_{out} = \frac{-S_{in}F}{\Delta S} \tag{3.2b}$$

where ΔS = S_{out} - S_{in}

3.2 Thermohaline circulation (THC)

Thermohaline circulation is a large-scale circulation that is driven by global density gradients created by surface heat and fresh water fluxes. Thermohaline refers to the temperature (thermo-) and dissolved salts (-haline) in ocean water.

In the Red Sea there are three water masses (three layers) involved in the thermohaline circulation (THC) at the strait of Bab el Mandab which are: surface water (SW), Gulf of Aden intermediate water (GAIW), Red Sea outflow water (RSOW) (Figure 1.1). The buoyancy forcing transform a warm fresh surface and intermediate inflow into cool saline outflow.

The THC model is simply an extension of the Kundsen equations that have been used to estimate estuarine circulation, by including the heat budget, as suggested by Eldevik and Nilsen (2010) for the exchange between North Atlantic and Arctic Mediterranean at Greenland-Scotland Ridge (GSR). We modify their model slightly. The result is Equations 3.3. In our Red Sea case we explicitly account for net evaporation in the volume budget, and salt is conserved.

$$U_1 + U_2 + U_3 = F \tag{3.3a}$$

$$S_1U_1 + S_2U_2 + S_3U_3 = 0 \tag{3.3b}$$

$$T_1U_1 + T_2U_2 + T_3U_3 = Q \tag{3.3c}$$

where F is the net evaporation, U_1 is the volume transport of the inflow at the surface (upper layer), U_2 is the volume transport of the inflow at the intermediate (intermediate layer), U_3 is the volume transport of the outflow at depth (lower layer), S_1 (T_1) is the salinity (temperature) of the upper layer, S_2 (T_2) is the salinity (temperature) of the intermediate layer, S_3 (T_3) is the salinity (temperature) of the lower layer, and Q is:

$$Q = \frac{Q'}{c_p \rho_0} \tag{3.4}$$

Q': heat transport in TW, ρ_0: density of sea water (= 1025 kg/m^3), c_p: is heat capacity of water(= 3986 J $K^{-1}kg^{-1}$) (Tragou et al., 1999).

To provide an estimate the annual mean evaporation rate F and the annual mean heat loss Q, we solved the system of Equation 3.3 by getting the value of the annual mean volume transport, temperature, and salinity from Table 3.2. First we solved Equation 3.3b with respect to U_2 to check consisting of Table 3.2, The result is 0.09 Sv in agreement with the tabulated values. Then from Equation 3.3a

the annual mean of evaporation is 20 mSv, and from Equations 3.3c and 3.4 the annual mean heat loss 8.5 TW:

$$F^{ref} = 20 \text{ mSv}, \quad Q^{ref} = 8.5 \text{ TW} \tag{3.5}$$

The net of evaporation and heat loss across the surface of the Red Sea per unit area is:

$$f^{ref} = F^{ref}/A = 1.4 \text{ m/yr} \tag{3.6a}$$
$$q^{ref} = Q^{ref}/A = 18.9 \text{ Wm}^{-2} \tag{3.6b}$$

$A = 0.45 \times 10^{12} \text{m}^2$ is the surface area of the Red Sea (Tragou et al., 1999).

Evaporation has been estimated by Neumann (1952) (2.15 m/yr), Privett (1959) (1.83 m/yr), Ahmad and Sultan (1987) (2.07 m/yr), and (da Silva et al., 1994) (1.50 m/yr). Our estimate is 1.4 m/yr, close to da Silva et al. (1994) but smaller than the other estimates. All estimates including methodologies are listed in Table 3.3.

Patzert (1974) estimated the annual mean heat loss from the surface of the Red Sea to 7 W m^{-2}. Ahmad and Sultan (1989) by using oceanic heat advection method 19 W m^{-2}, and by using bulk formula and by observations 22 W m^{-2}. Sofianos et al. (2002) found the annual mean heat loss 11.2 W m^{-2}. Our estimate for the heat loss, 18.9 W m^{-2}, is equivalent to Ahmad and Sultan (1989) when they used oceanic heat advection method. Table 3.4 shows these estimates for the annual mean heat loss from the surface of the Red Sea. Our estimates (Equations 3.6) are based on oceanic advection budgets.

TABLE 3.3: Estimates the net of evaporation from the surface of the Red Sea (Tragou et al., 1999) and (Sofianos et al., 2002).

Author	Method	f (m/yr)
Neumann (1952)	Bulk formula	2.15
Privett (1959)	Bulk formula	1.83
Ahmad and Sultan (1987)	Bulk formula	2.07
da Silva et al. (1994)	Bulk formula	1.50
f^{ref}	Oceanic salt advection	1.4

TABLE 3.4: Estimates of the annual mean heat loss from the surface of the Red Sea (Sofianos et al., 2002).

Author	Method	q (W m^{-2})
Patzert (1974)	Oceanic heat advection	7
Ahmad and Sultan (1989)	Oceanic heat advection	19
Sofianos et al. (2002)	Oceanic heat advection	11.2
Ahmad and Sultan (1989)	Bulk formula/observations	22
q^{ref}	oceanic heat advection	18.9

To solve the conservation equations (Eq. 3.3), we have to solve the system:

$$A\vec{U} = \vec{b} \tag{3.7}$$

where

$$A = \begin{pmatrix} 1 & 1 & 1 \\ S_1 & S_2 & S_3 \\ T_1 & T_2 & T_3 \end{pmatrix}$$

$$\vec{U} = \begin{pmatrix} U_1 \\ U_2 \\ U_3 \end{pmatrix}$$

$$\vec{b} = \begin{pmatrix} F \\ 0 \\ Q \end{pmatrix}$$

To get the volume transports we will solve

$$\vec{U} = A^{-1}\vec{b} \tag{3.8}$$

$A^{-1} = \frac{1}{det(A)} adj(A)$

Then the volume transports are:

$$U_1 = \frac{(S_2T_3 - S_3T_2)F - (S_2 - S_3)Q}{\Delta} \tag{3.9a}$$

$$U_2 = \frac{(S_3T_1 - S_1T_3)F - (S_3 - S_1)Q}{\Delta} \tag{3.9b}$$

$$U_3 = \frac{(S_1T_2 - S_2T_1)F - (S_1 - S_2)Q}{\Delta} \tag{3.9c}$$

where $\Delta = (S_1 - S_2)(T_1 - T_3) - (T_1 - T_2)(S_1 - S_3)$. Equations 3.9 are linear for the evaporation and heat loss.

The linear sensitivity of the volume transport to thermohaline change is given by partial derivatives. The partial derivatives of the surface inflow are:

$$\frac{\partial U_1}{\partial F} = \frac{S_2T_3 - S_3T_2}{\Delta} \tag{3.10a}$$

$$\frac{\partial U_1}{\partial Q} = \frac{S_3 - S_2}{\Delta} \tag{3.10b}$$

$$\begin{aligned}\frac{\partial U_1}{\partial T_1} &= \frac{(S_2 - S_3)Q - (S_2T_3 - S_3T_2)F}{\Delta^2}(S_3 - S_2) \\ &= -U_1\frac{\partial U_1}{\partial Q}\end{aligned} \tag{3.10c}$$

$$\begin{aligned}\frac{\partial U_1}{\partial S_1} &= \frac{(S_2 - S_3)Q - (S_2T_3 - S_3T_2)F}{\Delta^2}(T_2 - T_3) \\ &= \frac{-U_1(T_2 - T_3)}{\Delta}\end{aligned} \tag{3.10d}$$

The partial equations of volume transport of the intermediate and deep (U_2 and U_3) are similar.

Equation 3.10c can be written as:

$$\frac{\partial U_1}{\partial Q} = -\frac{1}{U_1}\frac{\partial U_1}{\partial T_1} \tag{3.11}$$

The change $\partial Q = -U_1 \partial T_1$ means decreasing surface temperature has the same effect as increasing heat loss from the surface. Quantitatively, Equation 3.11 means $U_1 \partial T_1$ provides the heat transport that can be compared directly with ∂Q.

The general expression of the change of volume transport for the three water masses with respect to water temperatures is:

$$\frac{\partial U_i}{\partial T_i} = -U_i \frac{\partial U_i}{\partial Q} \tag{3.12}$$

i = 1,2,3

And for salinities:

$$\frac{\partial U_i}{\partial S_i} = \frac{-U_i}{\Delta}(T_k - T_l) \tag{3.13}$$

i, k, l = 1,2,3 ; $k \neq l \neq i$

The other partial derivative equations in Appendix C.

Chapter 4

Results

In this chapter we will present the result of analytical models that constrain the change of the estuarine circulation and thermohaline circulation of the Red Sea using estuarine circulation model (equations 3.2) and THC model (equations 3.9).

4.1 Estuarine circulation

In this section we will show the result of the estuarine circulation at Bab el Mandab using estuarine circulation model, Equation 3.2, assuming reference salinities of inflow and outflow ($S_{in},\ S_{out}$), Section 3.1.

In winter (during October to May) there are two layer inverse estuarine exchange through the Bab el Mandab which are fresh water inflow on the top and a hypersaline outflow at the depth. This estuarine circulation illustrated by two layer model which are surface inflow and deep outflow.

4.1.1 Surface inflow

Figure 4.1 shows the volume transport (in Sv) of the surface inflow as a function of evaporation. We see that volume transport is direct proportional to evaporation, high volume transport with high evaporation.

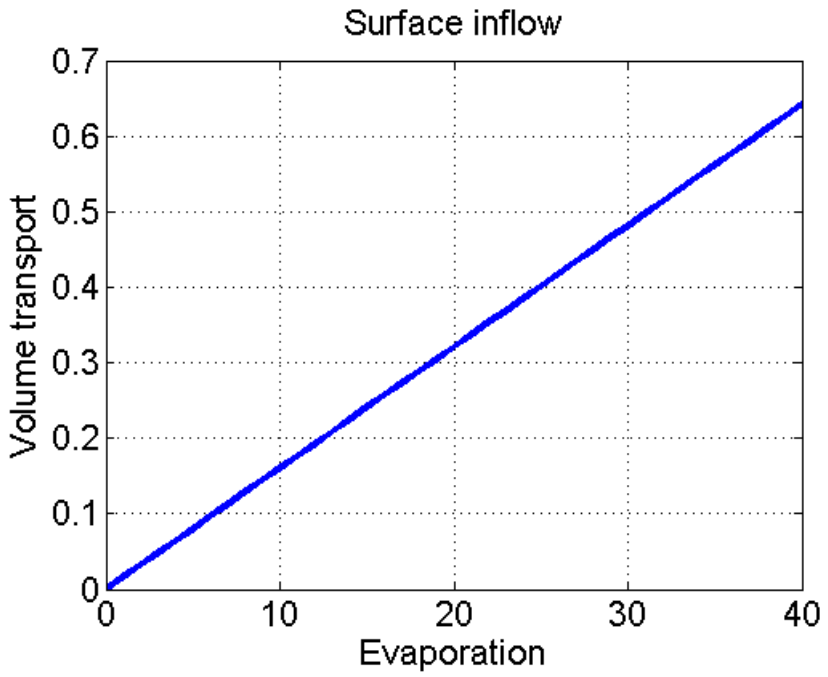

FIGURE 4.1: Volume transport (in Sv) of the surface inflow at Bab el Mandab.

4.1.2 Deep outflow

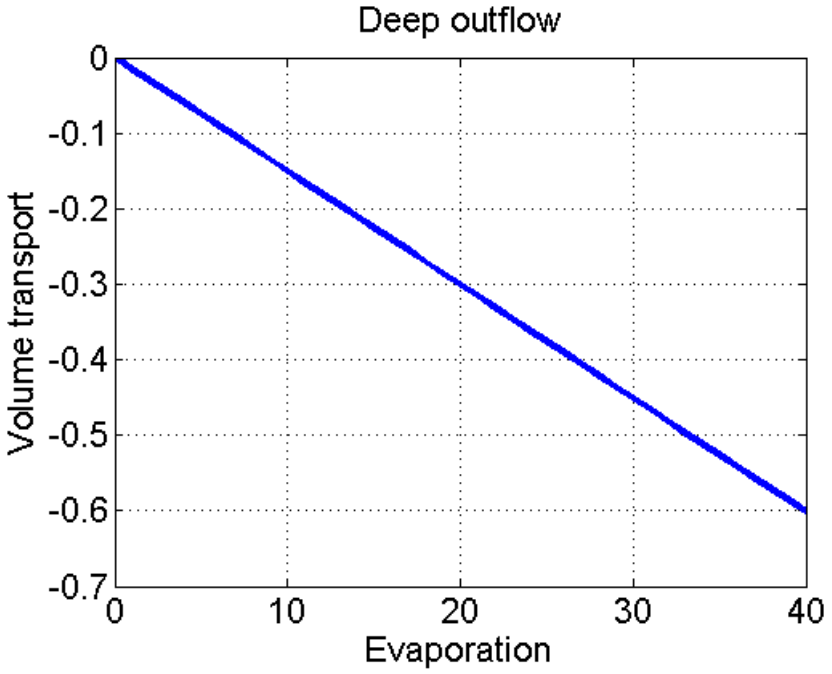

FIGURE 4.2: Volume transport (in Sv) of the deep outflow at Bab el Mandab.

Figure 4.2 shows the volume transport of the deep outflow changing with evaporation. In this figure, the volume transport increase when evaporation increase but in the opposite direction (out of the Red Sea).

This two layer model, however, represent the estuarine circulation model at Bab el Mandab. In the annual mean we will show the THC model for the three layer exchange through the Bab el Mandab strait.

4.2 THC model

The THC model, Equations 3.9, accounts for three layered exchange. As we mentioned in Figure 3.1, in the annual mean there are three layers at Bab el Manbab, upper layer (Surface Water SW) and intermediate layer (Gulf of Aden Intermediate Water GAIW) are going into the Red Sea, and the deep layer (Red Sea Outflow Water RSOW) going out of the Red Sea (to The Gulf of Aden).

We consider two cases for exchange at Bab el Mandab constrain by THC model, one assuming reference hydrography and variable buoyancy forcing, and the other with variable surface inflow hydrography (all else at reference values).

4.2.1 THC model constrained by evaporation and heat loss

In this section we represent the model as constrained by net evaporation (F) and heat loss (Q) assuming reference value of temperatures and salinities, Table 3.2.

Figures 4.3, 4.4, and 4.5 show the contour of volume transport in surface, intermediate, and depth, as function of evaporation and heat loss.

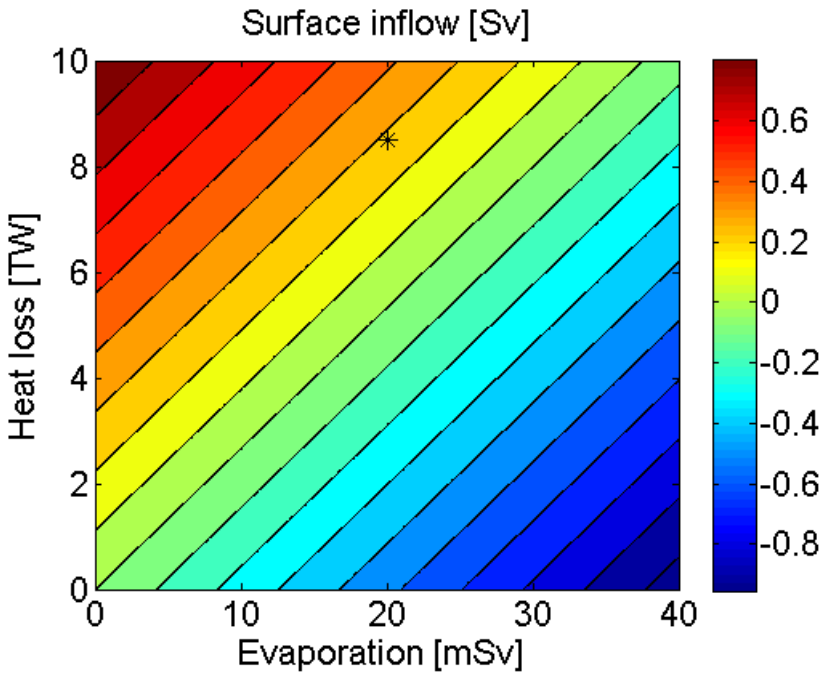

FIGURE 4.3: Contour of volume transport (in Sv) of the surface inflow constrained by evaporation and heat loss, (*) is reference evaporation and heat loss.

Figure 4.3 is the surface inflow. In this figure the volume transport decrease with increase evaporation, but in heat budget when the heat loss increase, the volume transport increase.

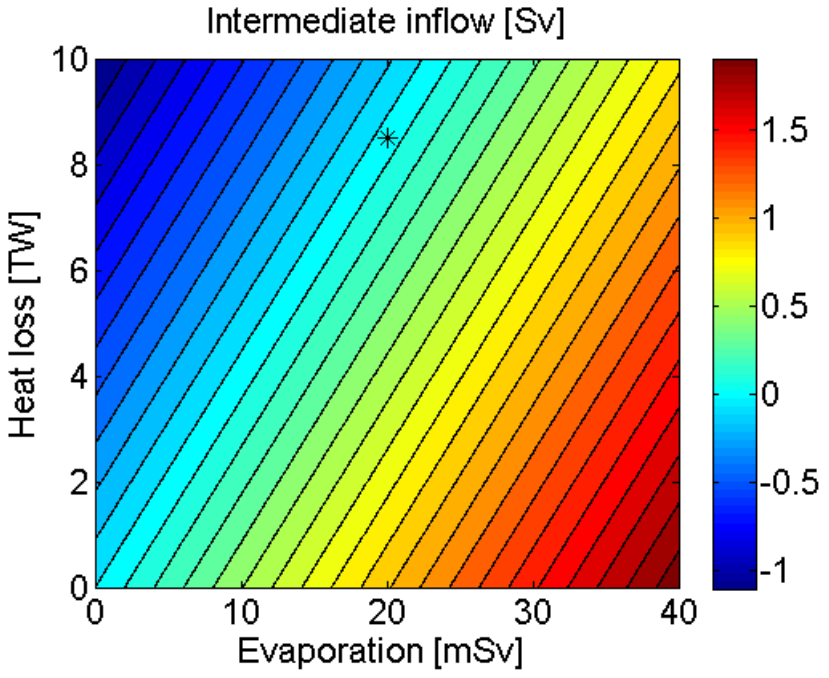

FIGURE 4.4: Contour of volume transport (in Sv) of the intermediate inflow constrained by evaporation and heat loss.

Figure 4.4 in intermediate inflow. This figure is opposite of the surface inflow figure; volume transport increases with evaporation and decreases with heat loss.

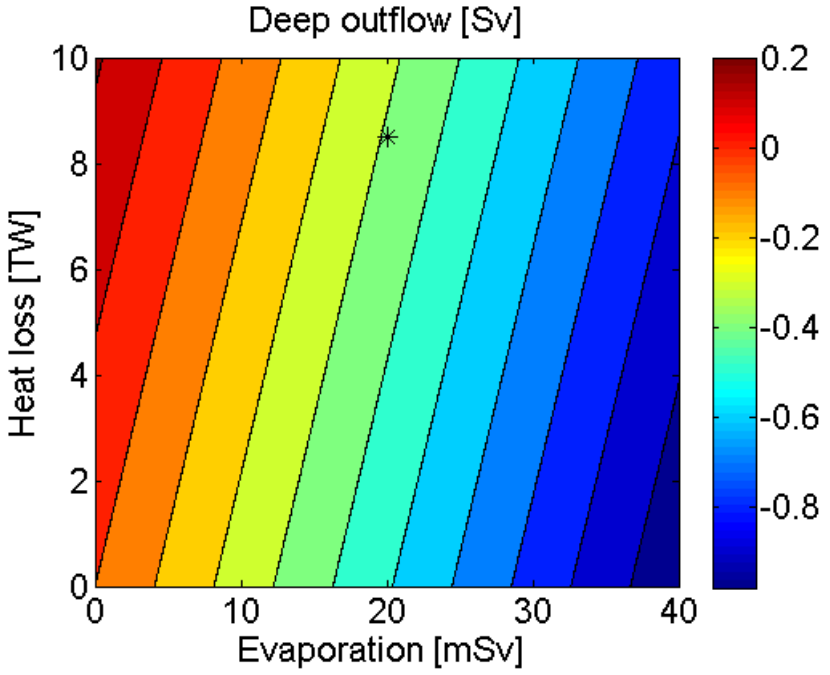

FIGURE 4.5: Contour of volume transport (in Sv) of the deep outflow constrained by evaporation and heat loss.

The deep outflow is show in Figure 4.5. In this figure we see volume transport decreases linearly with increased in evaporation, but it relatively insensitive to heat loss.

In Figures 4.3 and 4.4 we observed that the surface and intermediate inflow are sensitive to evaporation and heat loss, but intermediate is more sensitive. In Figure 4.5 the deep outflow is sensitive to evaporation.

Figures 4.3, 4.4, and 4.5 are possible mathematically. But physically $U_2 < 0$ and $U_3 > 0$ are imposible because intermediate layer (U_2) always going in to the Red Sea and the deep layer (U_3) is always going out. Figures 4.6, 4.7, and 4.8 consequently show the physically realizable THC model constrained by evaporation and heat loss.

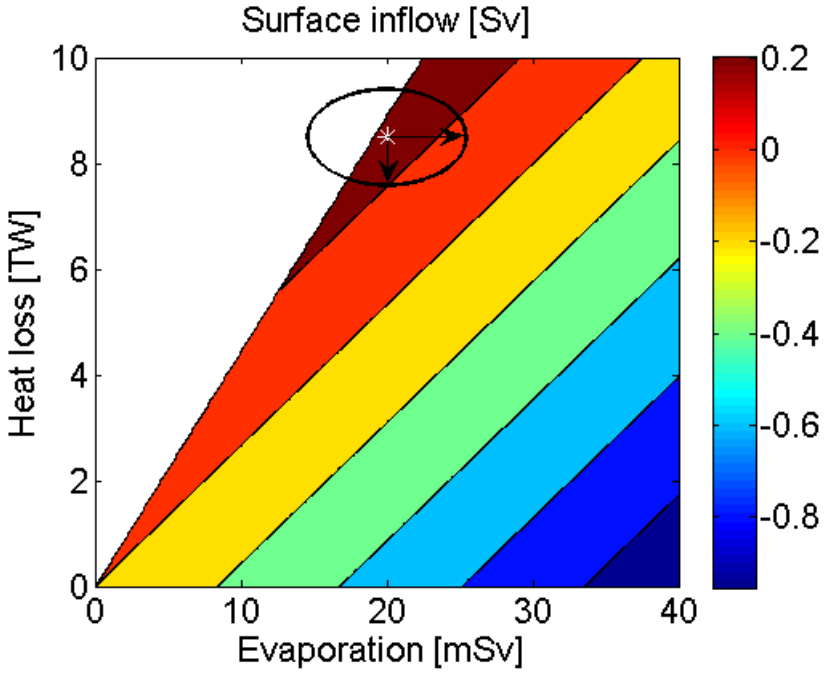

FIGURE 4.6: Model of exchange at Bab el Mandab in the surface inflow as function of evaporation and heat loss, the ellipse is an estimate of the observed range of variability.

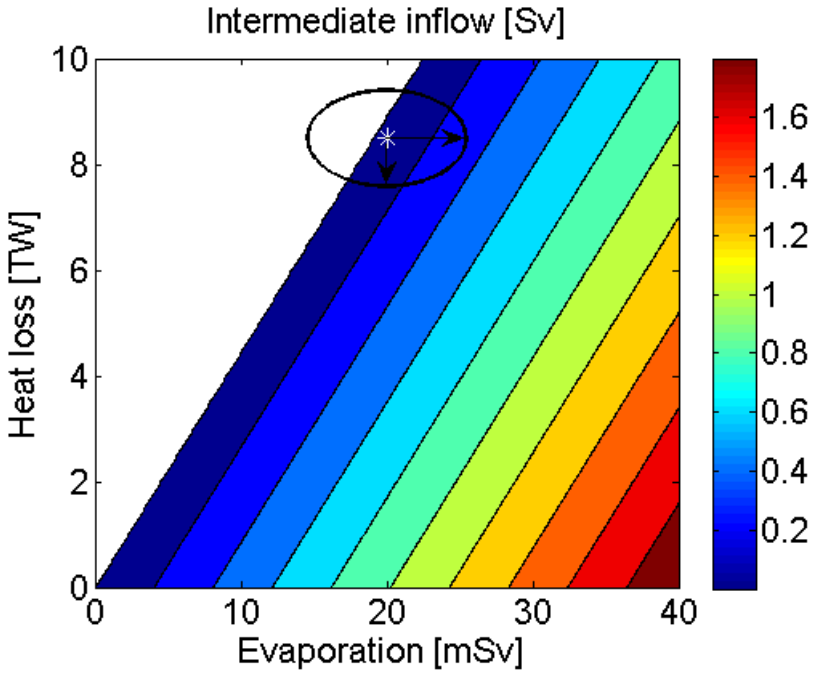

FIGURE 4.7: Model of exchange at Bab el Mandab in the intermediate inflow as function of evaporation and heat loss.

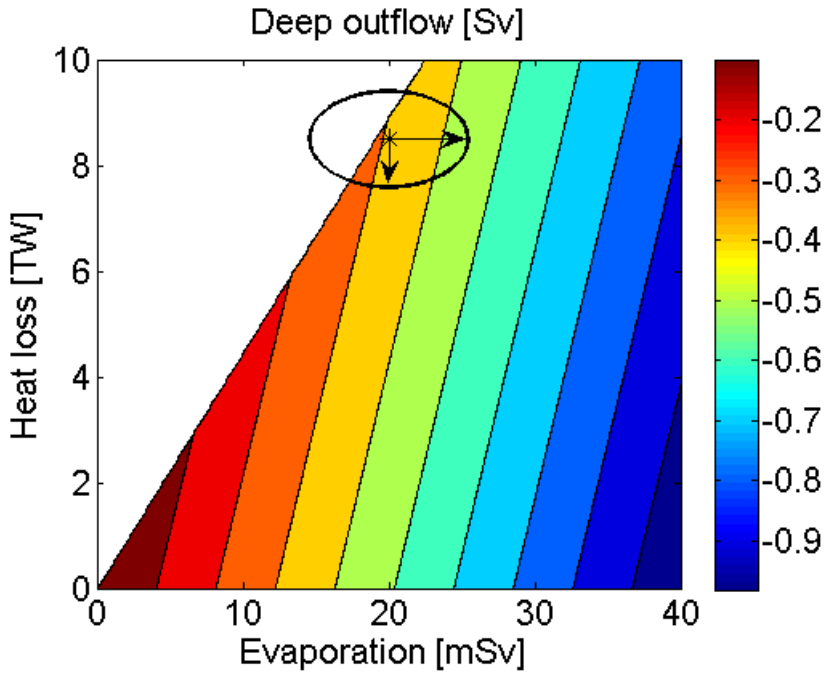

FIGURE 4.8: Model of exchange at Bab el Mandab in the deep outflow as function of evaporation and heat loss.

4.2.2 THC model constrained by surface salinity and temperature

In this section we will show the THC model as constrained by temperature and salinity of the surface.

Figures 4.9, 4.10, 4.11 display the contour of volume transport of the surface inflow, intermediate inflow, and deep outflow which are presented from the THC model equations, Equation 3.9, surface salinity and temperature are variables, and assuming reference temperatures and salinities of the intermediate and deep layers ($T_{2,3}$, $S_{2,3}$) from Table 3.2, and reference evaporation and heat loss from Equation 3.5.

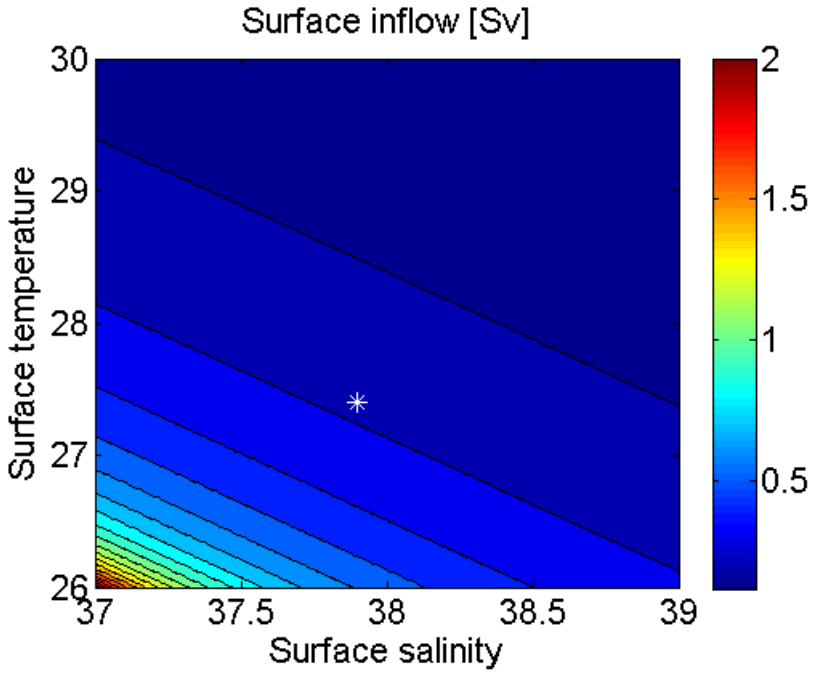

FIGURE 4.9: Contour of volume transport (in Sv) of the surface inflow constrained by temperature and salinity of the surface layer, (*) is reference surface salinity and temperature.

In Figure 4.9 volume transport of the surface inflow increase when salinity and temperature of the surface decrease.

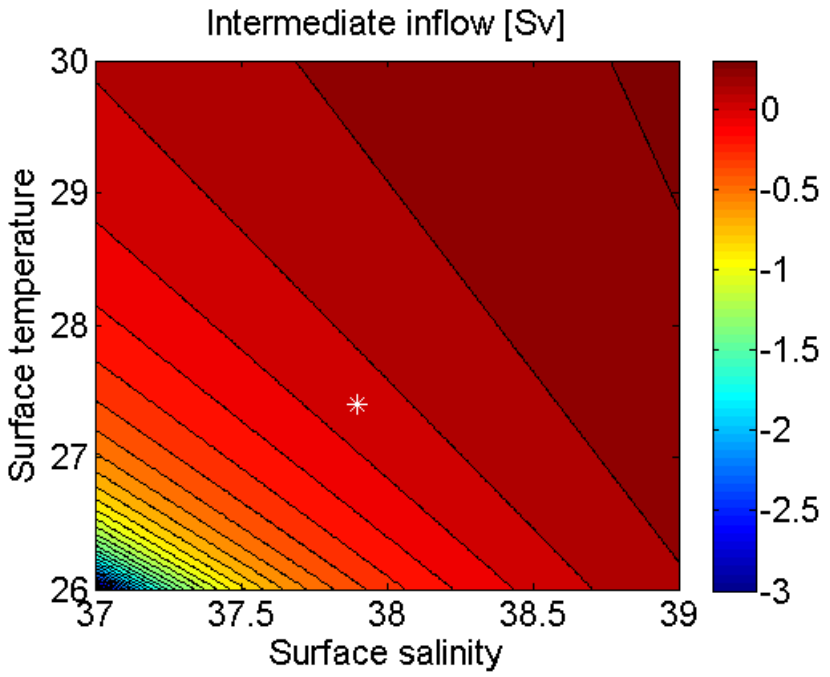

FIGURE 4.10: Contour of volume transport (in Sv) of the intermediate inflow constrained by temperature and salinity of the surface layer.

In Figure 4.10 we see direct proportional between volume transport and surface salinity, temperature, when surface salinity and temperature increase, volume transport of the intermediate inflow increase.

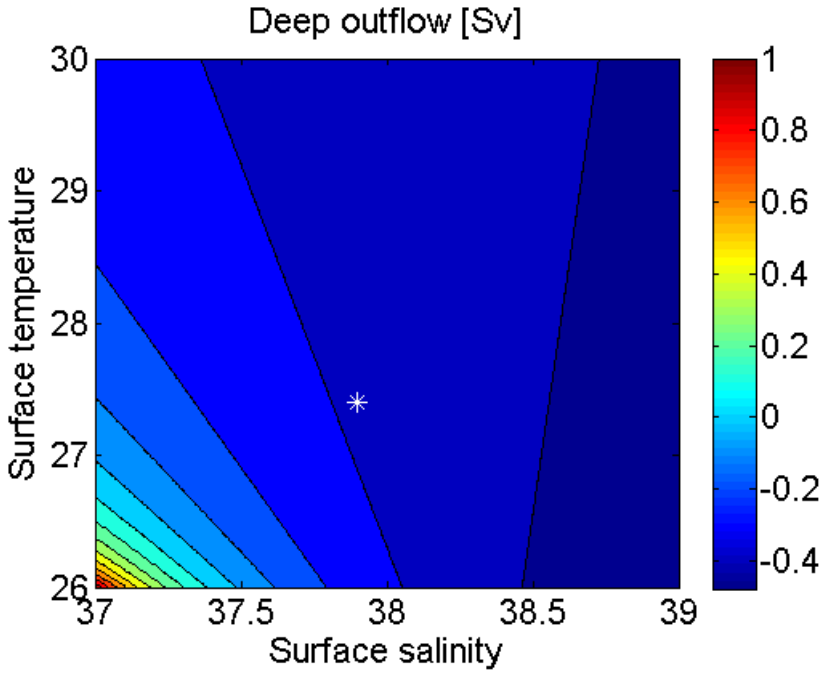

FIGURE 4.11: Contour of volume transport (in Sv) of the deep outflow constrained by temperature and salinity of the surface layer.

Figure 4.11 show the volume transport of the deep outflow. We see the volume transport decrease with increase salinity. And the volume transport decrease with increase temperature till salinity is about 38.4 psu, after that volume transport increase when temperature increase.

Physically, as we mentioned in Section 4.2.1 we have to remove U_2 (intermediate layer) < 0, and U_3 (deep layer) > 0. The result is displayed in Figures 4.12, 4.13, and 4.14.

Figures 4.12, 4.13, and 4.14 shows the THC model of the surface, intermediate, and deep layers which constrained by surface salinity and temperature.

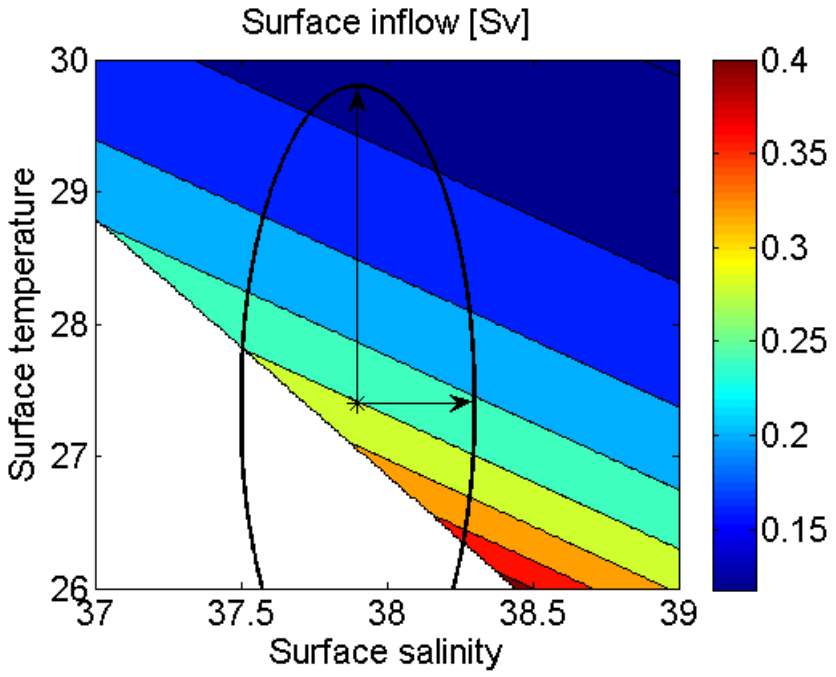

FIGURE 4.12: Model of volume transport (in Sv) of the surface inflow constrained by temperature and salinity of the surface layer, the ellipse is an estimate of the observed range of variability.

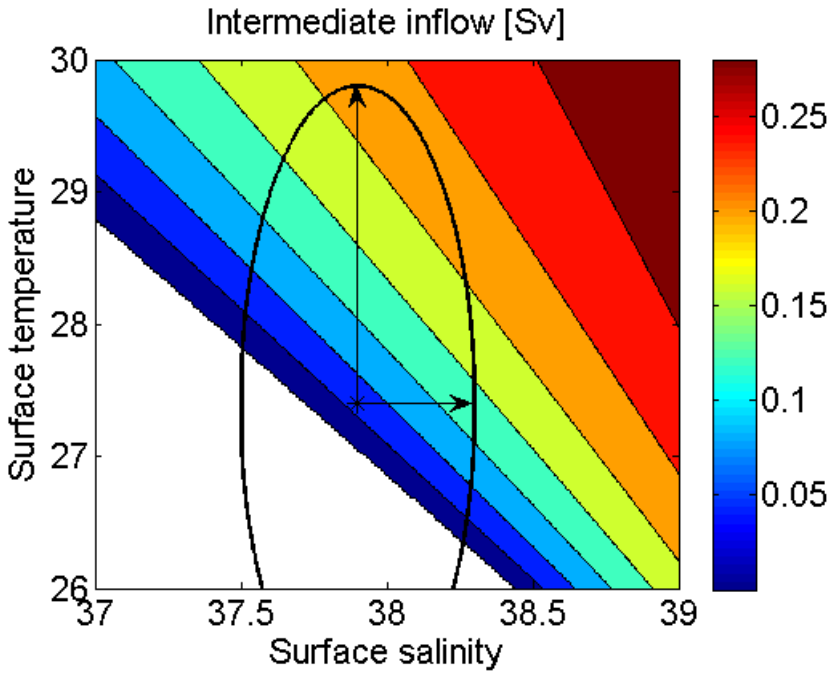

FIGURE 4.13: Model of volume transport (in Sv) of the intermediate inflow constrained by temperature and salinity of the surface layer.

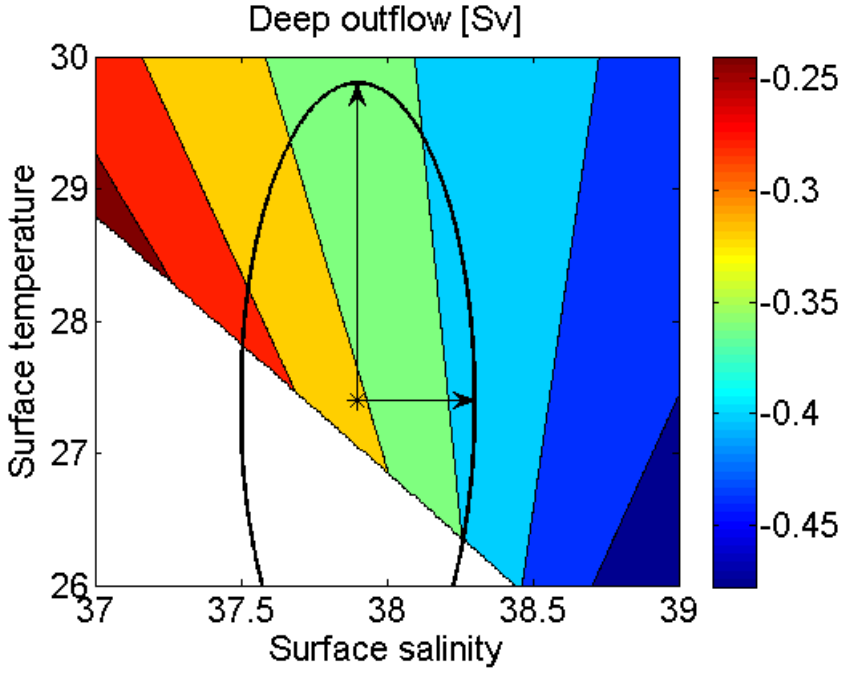

FIGURE 4.14: Model of volume transport (in Sv) of the deep outflow constrained by temperature and salinity of the surface layer.

Chapter 5

Discussion

In this thesis we used the thermohaline circulation model (THC) to constraine the volume transport of the sufrace, intermediate inflow and deep outflow as a function in buoyancy forcing and surface variables.

Figures 4.1 and 4.2 illustrate the estuarine circulation at Bab el Mandab strait, surface inflow and deep outflow are influenced by evaporation. As we mentioned preaviously in Chapter 1, estuarine circulation is drive by rate of evaporation.

The change in Figure 4.11 can explained geometrically from TS plot (Figure 3.2) as follow: If surface inflow fresher than intermediate inflow, then the deep outflow strong with increases surface temperature. If surface inflow saltier than intermediate inflow, deep outflow weak with increases surface temperature. And if surface and intermediate inflow have the same salinity , then the deep outflow constant when surface temperature increase.

Implication of the model

To show the implication of the THC model we will show the estimated range of the three water masses associated with the range of the evaporation and heat loss and compare with the previous studies and with the climate change.

Tragou et al. (1999) estimated the range of annual mean evaporation is $\pm$ 0.35 m/yr, and the heat loss is $\pm$ 2 W m^{-2}. And the estimate of Sofianos et al. (2002) is $\pm$ 0.22 m/yr for the range of the annual mean evaporation and $\pm$ 5

W m^{-2} for the heat loss. From Table 3.3 and 3.4 the range of the annual mean evaporation is $\pm$ 0.38 m/yr ($\pm$ 5.4 mSv) and the range of heat loss is $\pm$ 2 W m^{-2} ($\pm$ 0.9 TW). Our estimate is approach to Tragou et al. (1999) estimate.

According to THC model evaporation increase by 5.4 mSv and heat loss decrease by 0.9 TW. By taking the range of evaporation and heat loss then from the model (Figures 4.6, 4.7, and 4.8) the range of the volume transport of the surface inflow, intermediate inflow, and deep outflow is about 0.08 Sv, 0.04 Sv, and 0.06 Sv, and that is about 28%, 44%, 17% of the annual mean volume transport of the surface, intermediate and deep respectively. The largest range is in the surface.

Our modeled variability in Bab el Mandab exchange is in particular larger than the uncertainties associated with direct observation which are about (0.05 Sv, 0.01 Sv, 0.02 Sv) of the surface, intermediate, and deep respectively (Sofianos et al., 2002).

To show the range of the volume transport from the model which constrained by surface salinity and temperature, first we will get the range of the surface salinity and temperature from standard deviation of t_1 and s_1 from Table 3.1 and 3.2, the range is 2.4 °C, 0.4 psu, these estimates are relatively small compared with the range of temperature and salinity between the three water masses which are 3.2 °C, 1.7 psu . For the estimates of range of surface temperature and salinity, our model (Equations 3.10, C.1, C.2) associated the following range of the volume transport of the surface, intermediate, and deep layer are 0.15 Sv, 0.16 Sv , 0.16 Sv respectively, its larger than the range of volume transport in evaporation and heat loss case. The range of salinity transport (evaporation) and heat transport (heat loss) (in Figures 4.12, 4.13, 4.14) are about 3 mSv and 2.8 TW. In Figures (4.12, 4.13, 4.14) the range of temperature is three times larger than the heat loss in Figures (4.6, 4.7, 4.8).

For the possible future climate change, Fouda et al. (1994) used climate model and estimated the global mean temperature increased by 2 °C by the year 2030. And the estimated sensitivity for the African climate is 1.5 °C (Hulme et al., 2001), and by using climate model Hulme et al. (2001) estimate the range of temperature of the Red Sea by the year 2050 is about 1 °C. Hartmann (1994) estimated the sensitivity of heat flux from the tropical ocean by:

$$\frac{\Delta Q}{\Delta T} = 7 \text{ Wm}^{-2}\text{K}^{-1}$$

Since temperature increases by 1 °C (K), the increases of the heat loss is about 7 W m^{-2} (= 3.2 TW), it is increase by 37 % of the annual mean heat loss. From the model, Figures 4.6, 4.7, and 4.8, the volume transport of the surface is increase by about 0.2 Sv, and the intermediate decrease by about 0.2 Sv, and the deep decrease by about 0.07 Sv. We note that the possible future of the volume transport is larger than what was estimated for the considered range of variable buoyancy forcing (ellipses in Figures 4.6, 4.7, and 4.8). Increase the temperature by 1 °C is in the estimated range of surface variables (ellipses in Figures 4.12, 4.13, 4.14).

The expected temperature increase in the atmosphere would lead to increase in the Red Sea surface temperature and hence increase of evaporation (Fouda et al., 1994).

For the typical interannual variability in heat loss in the Red Sea Tragou and Garrett (1997) note that the interannual variability of the heat loss was increased from 1980 to early 1990 (based on data from 1947 to 1989) resulting primarily from increasing wind speed. This change in heat loss leads to change in evaporation and so the volume transport, but these change are relatively small (Smeed, 2004).

From the previous studies in the climate change, we note that the observational record indicate that the ocean basins, including the Red Sea, exhibit both warming and cooling over the last decades (Harrison and Carson, 2007).

Validity of the model

When we estabish our model, the underlying equations are conservation equations of the form:

$$\frac{\partial T}{\partial t} + \vec{U}. \bigtriangledown T = Q$$

This equation is conservation of heat, we neglected the variation in time (the first term) to set up THC model.

To esimate the time of the validity of our model, first we calculate how long time the Red Sea takes to renew the water. The volume transport of the Red Sea

(U) is about 0.37 Sv, and the volume of the Red Sea (V) is 2688×10^{11} m^3, then the time is:

$$\tau = \frac{V}{U} = 23\ yr$$

The estimate of time to renew the water from the basin is about 23 years. THC model works at the south of the Red Sea, the exchange across Bab el Mandab. We note that the time to renew all deep water of the Red Sea is estimated to be at least 40 years (Woelk and Quadfasel, 1996). This suggests that the THC model which are balance between ocean advection and external forcing is relevant and controlling for decadal scales.

In the equation model, Equation 3.3c, temperature transport balance by heat budget

$$U_1T_1 + U_2T_2 + U_3T_3 = Q^* + FT_1$$

we have omitted the last term which is the net loss of water through the surface of the Red Sea. From Table 3.2 and Equation 3.5, the neglected term is about 23% as it is 2 TW.

Chapter 6

Conclusions

In this thesis we modified Eldevik and Nilsen (2010) model to the thermohaline circulation of the Red Sea and constrained the exchange through the strait of Bab el Mandab. The model show the surface and intermediate inflow change with evaporation and heat budget, and the total thermohaline circulation, outflow, response to evaporation change, thus the model suggested the total circulation sensitive to evaporation. The model suggested that the circulation is relatively sensitive to thermohaline change (about 17% - 44% of the mean flow). As well as the model estimated a weaker thermohaline exchange at Bab el Mandab in 2050 using projected future climate change.

We note that the Strait of Hormuz connecting Arabian Gulf with the Gulf of Oman and Indian Ocean (Johns et al., 2003) also has a three-layered thermohaline exchange. Our THC model thus potentially be applied to constrain the exchange at the strait of Hormuz.

Appendix A

Matlab code

This Appendix provides MATLAB code that was used to plot estuarine circulation and thermohaline circulation model.

```
% load literaure values (Table 3.1)
MM=load('file.txt');

II = find(MM==0); % locate 0-values in data matrix;
MM(II) = NaN;     % by NaN (not-a-number)

% set reference hydrography
% 'nanmean' is 'mean' that ignore NaN-values
T1 = nanmean(MM(:,5));
T2 = nanmean(MM(:,6));
T3 = nanmean(MM(:,7));
S1 = nanmean(MM(:,8));
S2 = nanmean(MM(:,9));
S3 = nanmean(MM(:,10));

% define grid for unknowns F and Q
F = 0:.1:40;  % unit mSv
Q = 0:.01:10; % unit TW
[ff,qq]=meshgrid(F,Q);
```

```
cp = 4.1e3;  % specific heat capacity of seawater
rho0 = 1030; % reference density
convQ = cp*rho0/1e6; % To consitency with Sv
convF = 1e6/1e3;     % conversion from mSv to Sv

% Estuarine circulation plot

ut=S3*(F/convF)/(S3-S1);
ub=-S1*(F/convF)/(S3-S1);
figure;clf
plot(F,ut,'linewidth',3)
plot(F,ub,'linewidth',3)
grid on
set(gca,'fontsize',16)
xlabel('Evaporation')
ylabel('Volume transport')

% Thermohaline circulation plot
% calculate delta
s  = (S1-S2).*(T1-T3)-(T1-T2).*(S1-S3);
% calculate U1 and U2 inflow and U3 outflow
U1 = ((S2*T3-S3*T2)/s)*(ff/convF)-((S2-S3)/s)*(qq/convQ);
U2 = ((S3*T1-S1*T3)/s)*(ff/convF)-((S3-S1)/s)*(qq/convQ);
U3 = ((S1*T2-S2*T1)/s)*(ff/convF)-((S1-S2)/s)*(qq/convQ);

% contour plot of U1, U2 and U3

cvals = -1:.1:1;
figure;clf
contourf(ff,qq,U1,cvals)
contourf(ff,qq,U2,cvals)
contourf(ff,qq,U3,cvals)
colorbar
set(gca,'fontsize',16)
xlabel('Evaporation [mSv] ')
```

```
ylabel('Heat loss [TW]')
% Mark * to reference evaporation and heat loss
hold on
plot(20,8.5,'Marker','*','Color','k','MarkerSize',10)
hold off

% THC model plot constrain by evaporation and heat loss

% locate U2<0 and U3>0 in the matrix to NAN(not-a-number)
II=find(U2<0);
UU1=U1;
UU2=U2;
UU3=U3;
UU1(II)=NaN;
UU2(II)=NaN;
UU3(II)=NaN;

JJ=find(U3>0);
UU1(JJ)=NaN;
UU2(JJ)=NaN;
UU3(JJ)=NaN;
% make ellipse for the range of variability
dt = .01;
t = (dt:dt:10);
x = 5.4*sin(t) + 20;
y = .9*cos(t) + 8.5;

figure;clf
contourf(ff,qq,UU1)
contourf(ff,qq,UU2)
contourf(ff,qq,UU3)
colorbar
set(gca,'fontsize',16)
xlabel('Evaporation [mSv] ')
ylabel('Heat loss [TW]')
hold on
```

```
plot(20,8.5,'Marker','*','Color','w','MarkerSize',10)
plot(x,y,'LineWidth',2,'color','k')
hold off

% THC model contrain by surface temperature and salinity

% set reference hydrography

T2 = nanmean(MM(:,6));
T3 = nanmean(MM(:,7));
S2 = nanmean(MM(:,9));
S3 = nanmean(MM(:,10));

F = 20;   % unit mSv
Q = 8.5;  % unit TW

% define grid for unknowns T1 and S1

S1 = 37:.01:39;  % unit psu
T1 = 26:.01:30; % unit C
[ss,tt]=meshgrid(S1,T1);

s  = (ss-S2).*(tt-T3)-(tt-T2).*(ss-S3); % calculate delte
% calculate U1 and U2 inflow and U3 outflow
U1 = ((S2*T3-S3*T2)./s)*(F/convF)-((S2-S3)./s)*(Q/convQ);
U2 = ((S3*tt-ss*T3)./s)*(F/convF)-((S3-ss)./s)*(Q/convQ);
U3 = ((ss*T2-S2*tt)./s)*(F/convF)-((ss-S2)./s)*(Q/convQ);

% contour plot of U1, U2 and U3

figure;clf
cvals = -1:.1:2
contourf(ss,tt,U1,cvals)
colorbar
set(gca,'fontsize',16)
xlabel('Surface salinity')
```

```
ylabel('Surface temperature')
% Mark * to reference surface temperature and salinity
hold on
plot(37.9,27.4,'Marker','*','Color','w','MarkerSize',10)
hold off

% THC model constrain by surface temperature and salinity
% make ellipse for the range of variability
dt = .01;
t = (dt:dt:10);
x = .4*sin(t) + 37.9;
y = 2.4*cos(t) + 27.4;

cvals = -1:.04:1;
figure;clf
contourf(ss,tt,UU1,cvals)
colorbar
set(gca,'fontsize',16)
xlabel('Surface salinity')
ylabel('Surface temperature')
title('Surface inflow [Sv]')
hold on
plot(37.9,27.4,'Marker','*','Color','k','MarkerSize',10)
plot(x,y,'LineWidth',2,'color','k')
hold off
```

Appendix B

Statistics

Mean:

$$mean = \frac{\sum_{i=1}^{N} X_i}{N} \tag{B.1}$$

Standard deviation:

$$Std.\ dev. = \sqrt{\frac{\sum_{i=1}^{N} (X_i - \bar{X})^2}{N-1}} \tag{B.2}$$

Range:

$$range = X_{max} - X_{min} \tag{B.3}$$

Appendix C

Additional equations

This appendix provides additional partial derivatives equations of the volume transport with respect to temperature and salinities of the layers.

C.1 Partial derivatives with respect to temperature

$$\frac{\partial U_1}{\partial T_2} = \frac{-S_3 F}{\Delta} - U_1 \frac{\partial U_2}{\partial Q} \tag{C.1a}$$

$$\frac{\partial U_1}{\partial T_3} = \frac{S_2 F}{\Delta} - U_1 \frac{\partial U_3}{\partial Q} \tag{C.1b}$$

$$\frac{\partial U_2}{\partial T_1} = \frac{S_3 F}{\Delta} - U_2 \frac{\partial U_1}{\partial Q} \tag{C.1c}$$

$$\frac{\partial U_2}{\partial T_3} = \frac{-S_1 F}{\Delta} - U_2 \frac{\partial U_3}{\partial Q} \tag{C.1d}$$

$$\frac{\partial U_3}{\partial T_1} = \frac{-S_2 F}{\Delta} - U_3 \frac{\partial U_1}{\partial Q} \tag{C.1e}$$

$$\frac{\partial U_3}{\partial T_2} = \frac{S_1 F}{\Delta} - U_3 \frac{\partial U_2}{\partial Q} \tag{C.1f}$$

C.2 Partial derivatives with respect to salinity

$$\frac{\partial U_1}{\partial S_2} = \frac{(T_3F - Q) - U_1(T_3 - T_1)}{\Delta} \tag{C.2a}$$

$$\frac{\partial U_1}{\partial S_3} = \frac{(-T_2F + Q) - U_1(T_1 - T_2)}{\Delta} \tag{C.2b}$$

$$\frac{\partial U_2}{\partial S_1} = \frac{(-T_3F + Q) - U_2(T_2 - T_3)}{\Delta} \tag{C.2c}$$

$$\frac{\partial U_2}{\partial S_3} = \frac{(T_1F - Q) - U_2(T_1 - T_2)}{\Delta} \tag{C.2d}$$

$$\frac{\partial U_3}{\partial S_1} = \frac{(T_2F - Q) - U_3(T_2 - T_3)}{\Delta} \tag{C.2e}$$

$$\frac{\partial U_3}{\partial S_2} = \frac{(-T_1F + Q) - U_3(T_3 - T_1)}{\Delta} \tag{C.2f}$$

Bibliography

Ahmad, F. and Sultan, SAR (1987). On the heat balance terms in the central region of the Red Sea. *Deep Sea Research Part A. Oceanographic Research Papers*, **34**(10):pp. 1757–1760.

Ahmad, F. and Sultan, SAR (1989). Surface heat fluxes and their comparison with the oceanic heat flow in the Red Sea. *Oceanologica acta*, **12**(1):pp. 33–36.

Beal, L.M., Ffield, A., and Gordon, A.L. (2000). Spreading of Red Sea overflow waters. *Journal of geophysical research*, **105**(C4):pp. 8549–8564.

Britannica (2012). Gulf of aden. http://www.britannica.com/EBchecked/topic/5650/Gulf-of-Aden.

da Silva, A.M., Young, C.C., and Levitus, S. (1994). Atlas of surface marine data 1994. *Noaa atlas nesdis*, **6**(83):pp. 2910–3282.

Degens, E.T. and Ross, D.A. (1969). Hot brines and recent heavy metal deposits in the Red Sea. *New York, Springer-Verlag New York Inc.*

Eldevik, T. and Nilsen, J. (2010). Northern constraints on the Atlantic thermohaline circulation. Unpublished.

Fouda, M.M., Gerges, M.A., and Programme, United Nations Environment (1994). *Implications of climate change in the Red Sea and Gulf of Aden Region: an overview*. 99. United Nations Environment Programme.

Harrison, DE and Carson, M. (2007). Is the World Ocean warming? Upper-ocean temperature trends: 1950-2000. *Journal of physical oceanography*, **37**(2):pp. 174–187.

Hartmann, D.L. (1994). *Global physical climatology*, volume 56. Academic Pr.

Hulme, M., Doherty, R., Ngara, T., New, M., and Lister, D. (2001). African climate change: 1900-2100. *Climate Research*, **17**(2):pp. 145–168.

Jarosz, E. (1997). *Tidal dynamics in the Bab el Mandab Strait*. Ph.D. thesis, Faculty of the Louisiana State University and Agricultural and Mechanical College in partial fulfillment of the requirements for the degree of Doctor of Philosophy in The Department of Oceanography and Coastal Sciences by Ewa Jarosz MS, Louisiana State University.

Johns, WE, Yao, F., Olson, DB, Josey, SA, Grist, JP, and Smeed, DA (2003). Observations of seasonal exchange through the straits of Hormuz and the inferred heat and freshwater budgets of the Persian Gulf. *Journal of Geophysical Research*, **108**(C12):page 3391.

Levitus, S. and Boyer, T.P. (1994). World Ocean Atlas 1994. Volume 2. Oxygen. *Technical report*, National Environmental Satellite, Data, and Information Service, Washington, DC (United States).

Maillard, C. and Soliman, G. (1986). Hydrography of the Red Sea and exchanges with the Indian Ocean in summer. *Oceanologica acta*, **9**(3):pp. 249–269.

Morcos, S.A. (1970). Physical and chemical oceanography of the Red Sea. *Oceanography and Marine Biology: an annual review*, **8**:pp. 73–202.

Neumann, J. (1952). Evaporation from the Red Sea. *Israel Exploration Journal*, **2**(3):pp. 153–162.

Patzert, W.C. (1974). Volume and heat transports between the Red Sea and the Gulf of Aden, and notes on the Red Sea heat Budget. In: *International Association of Physical Science Ocean (IAPSO) Symposium Physical Oceanography of the Red Sea SCOR and UNESCO, Paris*. (pp. 191–201).

Privett, DW (1959). Monthly charts of evaporation from the N. Indian Ocean (including the Red Sea and the Persian Gulf). *Quarterly Journal of the Royal Meteorological Society*, **85**(366):pp. 424–428.

Saad, A. M. E (2010). *Wave and wind conditions in the Red Sea A numerical study using a third generation wave model*. Master's thesis, University of Bergen.

Schott, F.A. and McCreary Jr, J.P. (2001). The monsoon circulation of the Indian Ocean. *Progress in Oceanography*, **51**(1):pp. 1–123.

Siddall, M., Smeed, DA, Mathiessen, S., and Rohling, EJ (2002a). Exchange flow between the Red Sea and the Gulf of Aden. In: *The 2nd Meeting on the Physical Oceanography of Sea Straits, Villefranche*. (pp. 203–6).

Siddall, M., Smeed, D.A., Matthiesen, S., and Rohling, E.J. (2002b). Modelling the seasonal cycle of the exchange flow in Bab el Mandab (Red Sea). *Deep Sea Research Part I: Oceanographic Research Papers*, **49**(9):pp. 1551–1569.

Smeed, D.A. (2004). Exchange through the Bab el Mandab. *Deep Sea Research Part II: Topical Studies in Oceanography*, **51**(4-5):pp. 455–474.

Sofianos, S.S. and Johns, W.E. (2002). An Oceanic General Circulation Model (OGCM) investigation of the Red Sea circulation, 1. Exchange between the Red Sea and the Indian Ocean. *Journal of geophysical research*, **107**(C11):page 3196.

Sofianos, SS, Johns, WE, and Murray, SP (2002). Heat and freshwater budgets in the Red Sea from direct observations at Bab el Mandeb. *Deep Sea Research Part II: Topical Studies in Oceanography*, **49**(7-8):pp. 1323–1340.

Tragou, E. and Garrett, C. (1997). The shallow thermohaline circulation of the Red Sea. *Deep Sea Research Part I: Oceanographic Research Papers*, **44**(8):pp. 1355–1376.

Tragou, E., Garrett, C., Outerbridge, R., and Gilman, C. (1999). The heat and freshwater budgets of the Red Sea. *Journal of physical oceanography*, **29**(10):pp. 2504–2522.

Wikipedia (2012). Red Sea topographic map. http://en.wikipedia.org/wiki/File:Red_Sea_topographic_map-en.jpg.

Woelk, S. and Quadfasel, D. (1996). Renewal of deep water in the Red Sea during 1982-1987. *Journal of Geophysical research-all series-*, **101**(C8):pp. 18,155–18,165.